JACS
JOURNAL OF THE AMERICAN CHEMICAL SOCIETY
Article
pubs.acs.org/JACS

Effects of Electron Trapping and Protonation on the Efficiency of Water-Splitting Dye-Sensitized Solar Cells

John R. Swierk, Nicholas S. McCool, Timothy P. Saunders, Greg D. Barber, and Thomas E. Mallouk*

Department of Chemistry, The Pennsylvania State University, University Park, Pennsylvania 16802, United States

Supporting Information

ABSTRACT: Water-splitting dye-sensitized photoelectrochemical (WS-DSPECs) cells employ molecular sensitizers to absorb light and transport holes across the TiO_2 surface to colloidal or molecular water oxidation catalysts. As hole diffusion occurs along the surface, electrons are transported through the mesoporous TiO_2 film. In this paper we report the effects of electron trapping and protonation in the TiO_2 film on the dynamics of electron and hole transport in WS-DSPECs. When the sensitizer bis(2,2′-bipyridine)(4,4′-diphosphonato-2,2′-bipyridine)-ruthenium(II) is adsorbed from aqueous acid instead of from ethanol, there is more rapid hole transfer between photo-oxidized sensitizer molecules that are adsorbed from strong acid. However, the photocurrent and open-circuit photovoltage are dramatically lower with sensitizers adsorbed from acid because intercalated protons charge-compensate electron traps in the TiO_2 film. Kinetic modeling of the photocurrent shows that electron trapping is responsible for the rapid electrode polarization that is observed in all WS-DSPECs. Electrochemical impedance spectroscopy suggests that proton intercalation also plays an important role in the slow degradation of WS-DSPECs, which generate protons at the anode as water is oxidized to oxygen.

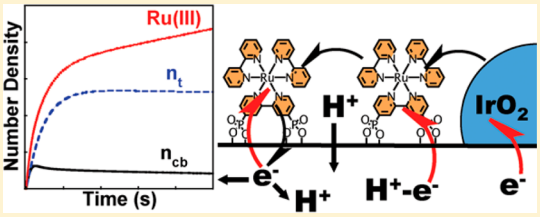

INTRODUCTION

The efficient conversion of sunlight to stored energy in fuels is a key challenge for solar energy research. Water-splitting dye-sensitized photoelectrochemical cells (WS-DSPECs) use a modular, component-based approach to drive water-splitting under visible light illumination. In these cells, a mesoporous anatase TiO_2 anode is sensitized with a dye and a water oxidation catalyst. Under illumination, the photoexcited dye injects an electron into the conduction band of the TiO_2 and is subsequently reduced by the catalyst, which oxidizes water to generate oxygen and protons. The TiO_2 electrode transports electrons through a circuit to a dark catalytic cathode where protons are reduced to hydrogen.[1]

While incident photon-to-current efficiencies up to 15% have been reported in DS-WSPECs,[2] most combinations of sensitizers and water oxidation catalysts give relatively low photocurrents. Almost invariably, the photocurrent decays over a period of seconds to minutes. However, most of the initial photocurrent can be restored by holding the cell in the dark for a few seconds. So far, this rapid polarization and dark recovery of the photoanode in WS-DSPECs has not been adequately explained.

Fast transport of photoinjected electrons through TiO_2 is a crucial parameter for efficient operation of conventional dye-sensitized solar cells. In nanocrystalline TiO_2 films, trap states are thought to be the related to crystallographically misaligned crystallites at the particle/particle interface. These states have an exponential distribution in energy below the conduction band edge.[3] Electron diffusion coefficients in nanocrystalline TiO_2 are several orders of magnitude lower than in single crystals.[4] In aqueous environments, proton intercalation stabilizes reduced Ti(III) sites,[5,6] leading to the formation of energetically shallow, long-lived trap states that retard transport.[7] Proton intercalation decreases the electron diffusion coefficient by an at least one additional order of magnitude.[7]

Electrochemical studies of WS-DSPECs have shown that electron self-exchange between adsorbed sensitizer molecules is also a key kinetic parameter.[8−10] Following photoexcitation and electron injection into TiO_2, the hole on the sensitizer molecule moves across the surface in a series of lateral transfers until it recombines with an electron or encounters a water oxidation catalyst particle. Because the catalyst surface coverage is typically very low (pmol/cm^2) and hole transport is slow, only a fraction of the electrode surface is active for photoelectrochemical water oxidation.

An additional complication in WS-DSPECs is desorption of the sensitizer into the aqueous electrolyte. Most studies to date have used ruthenium polypyridyl complexes as sensitizers.[2,11−14] Thermodynamically, ruthenium tris(bipyridyl) derivatives are able to inject an electron into the conduction band of TiO_2 at pH < 10 and oxidize water at pH > 4.5.[1] Desorption of these sensitizers results in a progressive decay in photocurrent.[15] High potential porphyrins are insoluble in water and have also been studied as sensitizers in WS-DSPECs,[3,16,17] but so far their hole transport kinetics have not been studied.

A number of earlier studies have measured electron transport and recombination rates[18−23] in nonaqueous dye-sensitized solar cells as well as the specific role of intercalated protons in

Received: April 23, 2014
Published: July 14, 2014

   dx.doi.org/10.1021/ja5040705 | J. Am. Chem. Soc. 2014, 136, 10974−10982

electron transport within TiO_2.[5,7] In this paper we extend those techniques to WS-DSPECs to provide insight into the factors that limit their efficiency. These measurements provide an explanation for the decay in photocurrent over seconds to minutes that has been so far observed in all examples of WS-DSPECs. We compare WS-DSPECs in which a ruthenium polypyridyl sensitizer has been adsorbed onto nanocrystalline TiO_2 from either nonaqueous or acidic aqueous solutions. The choice of solvent used in the sensitization process profoundly affects the photoelectrochemistry by changing the rate of lateral hole transfer and the trapping of electrons in the TiO_2 film. Spectroelectrochemical measurements demonstrate that proton intercalation during sensitization significantly affects the photoelectrochemical behavior of WS-DSPECs. A kinetic model that incorporates terms for the trapping of photoinjected electrons, charge recombination, and catalytic water oxidation successfully explains photocurrent decay. Electrochemical impedance spectroscopy reveals capacitive effects associated with intercalated protons in cells that have undergone photoelectrolysis, suggesting that proton intercalation plays a role in the long term photocurrent decay associated with WS-DSPECs.

EXPERIMENTAL SECTION

Bis(2,2′-bipyridine)(4,4′-diphosphonato-2,2′-bipyridine)ruthenium bromide (Figure 1, $[Ru(bpy)_2(4,4'\text{-}(PO_3H_2)_2bpy)]$) was synthesized and purified as reported by Gillaizeau-Gauthier et al.[4,24]

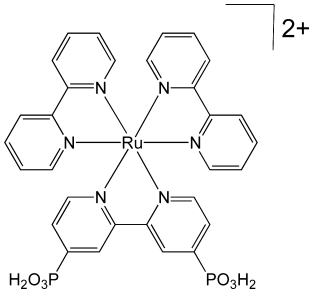

Figure 1. Structure of bis(2,2′-bipyridine)(4,4′-diphosphonato-2,2′-bipyridine)ruthenium(II).

Photoanode Preparation. Colloidal anatase TiO_2 suspensions[5,6,25] and TiO_2 photoanode films were prepared as previously described.[7,26] Briefly, a colloidal TiO_2 suspension was doctor-bladed onto 8Ω/cm^2 fluorine-doped tin oxide-coated glass (FTO-glass, Hartford Glass Company) and sintered to form a 12 μm thick film. Electrodes used for photoelectrochemical studies were catalyzed by soaking in 100 μM citrate-capped IrO_x for 14 h before sintering at 450 °C for 3 h.[26] The electrodes were sensitized in the dark by soaking in a solution of sensitizer for 22 h, rinsed thoroughly with clean solvent, dried under a stream of N_2, and stored in the dark. The quality of the TiO_2 films was assessed by testing the electrodes in conventional nonaqueous dye-sensitized solar cells (see Supporting Information).

Absorption spectra were recorded on a Cary 6000i (Agilent) UV–vis spectrophotometer by placing a dry electrode perpendicular to the beam path. The spectra were blanked to a bare piece of FTO-glass. For surface coverage measurements, scattering from the TiO_2 film was compensated by using a bare TiO_2 electrode as a blank.

Electrochemical Characterization. Cyclic voltammetry (CV) of dye-sensitized electrodes was performed in 0.1 M $LiClO_4$ in acetonitrile using a Nuvant EZ-Stat Pro potentiostat at a scan rate of 10 mV s^{-1}. The potential was applied relative to a nonaqueous Ag/Ag$^+$ (0.01 M $AgNO_3$ in 0.1 M TBAP, Bioanalytical Systems, Inc.) reference electrode.

Cross-Surface Electron Diffusion Constant (D_{app}). Following the method of Hanson et al.,[7,10] D_{app} was measured in 0.1 M $HClO_4$ (aq) by applying a potential of 1.5 V vs Ag/AgCl (3.5 M NaCl) for 10 min, then 0.0 V for an additional 10 min. D_{app} was calculated by monitoring the change in absorbance at 490 nm and then analyzing the data according to eq 1:

$$\Delta A = \frac{2A_{max}D_{app}^{1/2}t^{1/2}}{d\pi^{1/2}} \quad (1)$$

Here ΔA is the change in absorbance ($A_{max} - A(t)$), t is the time in seconds, and d is the thickness of the film (12 μm). D_{app} was determined by fitting the change in absorbance to eq 1 over the first 1.5 min.

Photoelectrochemical Characterization. Steady state photoelectrochemical measurements were made in 0.1 M NaH_2PO_4/Na_2HPO_4 buffer (pH 6.8) at 100 mV vs Ag/AgCl (3.5 M NaCl) using a Nuvant EZ-Stat Pro potentiostat. Photocurrents were typically recorded over a period of 10 min. Chronopotentiometry was performed under zero current conditions with a Metrohm Autolab potentiostat, with potentials measured relative to the Ag/AgCl (3.5 M NaCl) reference electrode. In each deposition solvent, the concentration of sensitizer was adjusted so that the anode had an absorbance of 1.1 to 1.2 at 460 nm. The photoanode and reference electrode were placed in one compartment of an H-cell and sealed with a septum. The cathode (Pt mesh electrode) was placed in the adjacent compartment, also sealed with a septum, and purged with 5% hydrogen in argon. The anode was illuminated with a 150 W Newport Oriel Lamp with AM 0, AM 1.5 and 410 nm long-pass filters.

Electrochemical impedance spectroscopy was performed in a three-electrode configuration in galvanostatic mode. A Metrohm Autolab potentiostat with a FRA32 M module provided a 3 μA perturbation on top of a constant current of 0.0 μA. To ensure that the sample was stable over the time scale of the experiment, the frequency range measured was 1 MHz to 10 Hz.

RESULTS AND DISCUSSION

Surface Adsorption of Sensitizer Molecules. Table 1 shows the results of adsorption experiments conducted with the $[Ru(bpy)_2(4,4'\text{-}(PO_3H_2)_2bpy)]$ sensitizer in different solvents. Saturation surface coverages (Γ_{max}) and adsorption equilibrium constants (K_{ad}) were calculated from the data using a Langmuirian model (Figure S2, Supporting Information). Films of TiO_2 on FTO-glass were soaked in 10, 20, 50, 100, 150, and 200 μM $[Ru(bpy)_2(4,4'\text{-}(PO_3H_2)_2bpy)]$ for 22 h. Surface coverages were measured from the absorbance of the dry film at 454 nm using eq 2:[10]

Table 1. Surface Binding Parameters As a Function of Deposition Solvent Obtained from a Langmuirian Fit of Surface Coverage As a Function Dye Concentration

deposition solvent	Γ_{max} (10^{-7} mol cm^{-2})	K_{ad} (10^4 M^{-1})
0.1 M $HClO_4$ (aq)	1.2 ± 0.1	1.8 ± 0.5
H_2O	1.4 ± 0.4	0.9 ± 0.4
DMSO	0.9 ± 0.1	0.9 ± 0.3
ethanol	2.0 ± 0.4	0.7 ± 0.3

$$\Gamma(\text{mol cm}^{-2}) = \frac{A(\lambda)/\varepsilon(\lambda)}{1000} \quad (2)$$

Recently, we determined the surface area of these TiO_2 films to be 98.2 m^2/g or 1120 cm^2 per cm^2 of geometric area.[26] The equilibrium adsorption constant obtained when depositing from 0.1 M $HClO_4$ (aq), 1.8 × 10^4 M^{-1} (Table 1), is in agreement with the value measured by Hanson et al. (1.7 × 10^4

dx.doi.org/10.1021/ja5040705 | J. Am. Chem. Soc. 2014, 136, 10974–10982

M^{-1}).[10] In other solvents, K_{ad} is lower by approximately a factor of 2. The saturation surface coverage for different deposition solvents does not follow the trend in K_{ad}. Films prepared from ethanol had the highest saturation coverage at 2.0×10^{-7} mol cm^{-2} and films prepared from DMSO had roughly half that value.

Qu and Meyer[27] as well as Kim et al.[28] observed similar behavior with carboxylate derivatives of ruthenium polypyridyl complexes on TiO_2. The sensitizers adsorbed rapidly to TiO_2 pretreated in acid, but the saturation coverage was only ~1/3 that of of base-pretreated films. These results may be rationalized in terms the overall charge on the complex. At low pH the phosphonic acids groups should be fully protonated[29] giving the complex an overall charge of +2. In aqueous 0.1 M $HClO_4$, as the surface coverage increases, electrostatic repulsion between free and bound sensitizer cations is expected to limit the surface coverage. This is reminiscent of layer-by-layer chemistry where polyelectrolytes deposit to a self-limiting thickness controlled by electrostatic repulsion.[30] In unbuffered water and nonaqueous solvents, the protonation state of the phosphonic acid groups is not known precisely. The complex could be cationic, neutral, or anionic with a maximum charge of −2; in low dielectric solvents such as DMSO, ion pairing may also occur. In these cases it is likely that there is less electrostatic repulsion between free and adsorbed sensitizer molecules, allowing for higher surface coverage.

Surface Electrochemistry. The cyclic voltammagram (CV) of $[Ru(bpy)_2(4,4'\text{-}(PO_3H_2)_2bpy)]$ deposited from 0.1 M $HClO_4$ (aq) on TiO_2 shows a single, well-defined peak at $E_{1/2}$ =0.85 V vs Ag/Ag^+ (Figure 2). Although the peaks are

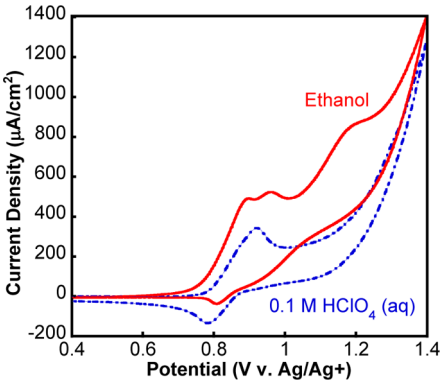

Figure 2. Cyclic voltammetry of TiO_2 films (without IrO_2) sensitized from 200 μM $[Ru(bpy)_2(4,4'\text{-}(PO_3H_2)_2bpy)]$ in ethanol (red, Γ = 1.04×10^{-7} mol cm^{-2}) and 0.1 M $HClO_4$ (aq) (blue, Γ = 8.66×10^{-8} mol cm^{-2}) in 0.1 M $LiClO_4$/acetonitrile versus a nonaqueous Ag/Ag^+ reference electrode (Fc/Fc^+ = 0.1 V vs Ag/Ag^+).

somewhat broadened ($E_{pa} - E_{pc}$ = 0.14 V), the single quasi-reversible wave indicates a low degree of aggregation. This is consistent with the picture of electrostatic repulsion between charged sensitizer molecules. In contrast, the CV of a sensitized electrode prepared from ethanol shows several overlapping and broad waves. A reversible wave can be observed at $E_{1/2}$ = 0.85 V vs Ag/Ag^+ along with a quasi-reversible wave at 0.93 V. A third irreversible wave is observed at 1.2 V. The peak-to-peak separation of the wave at 0.85 V is smaller than that in the 0.1 M $HClO_4$ (aq) prepared samples. However, the complexity of the CV suggests that the sensitizer does not cover the TiO_2 in a uniform monolayer; instead, there appear to be patches of monolayer coverage as well as sensitizer aggregation. This supports the picture of neutral or weakly charged sensitizers that do not repel each other in the adsorption process.

Films prepared from DMSO and H_2O show an irreversible wave at 0.84 V vs Ag/Ag^+ (Figure S3, Supporting Information). A second irreversible wave is observed at 0.92 and 0.94 V in the DMSO and H_2O CVs, respectively, with a third irreversible wave at 1.1 V in the H_2O CV. The irreversibility and multiplicity of anodic waves suggest significant dye aggregation in these films.

Cross-Surface Hole Transfer. D_{app} was measured for TiO_2 films sensitized with $[Ru(bpy)_2(4,4'\text{-}(PO_3H_2)_2bpy)]$ as a function of sensitizer coverage and deposition solvent (Figure 3). The highest D_{app} values were obtained with electrodes

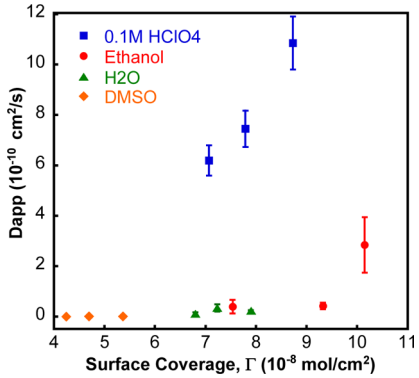

Figure 3. Cross-surface hole diffusion coefficient (D_{app}) vs sensitizer coverage for electrodes prepared from different solvents.

sensitized in 0.1 M $HClO_4$ (aq). The value measured at the highest coverage ($11 \pm 1 \times 10^{-10}$ cm^2/s, Figure 3) is in good agreement with the previously reported value (13.3×10^{-10} cm^2/s).[10] D_{app} was roughly an order of magnitude lower ($3 \pm 1 \times 10^{-10}$ cm^2/s) for films prepared at similar sensitizer coverage in ethanol and other solvents. Qu and Meyer observe a similar increase in the rate of cross-surface electron transfer for carboxylic acid functionalized sensitizers on proton treated TiO_2.[27] In that study, they suggested that small, interfacial cations may help to lower reorganization energy or that protonation may lead to a difference in binding mode (monodentate versus bidentate).

Interestingly, D_{app} increases significantly at the highest coverage (1.0×10^{-7} mol/cm^2) for films prepared from ethanol. Since Langmuir isotherms (Figure S1, Supporting Information) show that these films have not attained saturation coverage, it may be interesting to investigate higher coverage films, e.g., with polymeric ruthenium polypyridyl sensitizers adsorbed from ethanol. This suggests that in the absence of protonation, the percolation threshold for $[Ru(bpy)_2(4,4'\text{-}(PO_3H_2)_2bpy)]$ to efficiently shuttle electrons across the surface of TiO_2 is $\sim 1 \times 10^{-7}$ mol cm^{-2}. The percolation threshold for efficient cross-surface electron in the presence of protonation appears to be significantly lower, consistent with observations of related systems.[31−33]

Proton Intercalation during Sensitization. Figure 4 shows transient open-circuit photovoltages for dye-sensitized electrodes, measured by chronopotentiometry. In WS-DSPECs the photovoltage is the potential difference between the Fermi level of the TiO_2 under illumination and the potential of the O_2/H_2O couple at the relevant pH.[26] Under illumination, the

dx.doi.org/10.1021/ja5040705 | J. Am. Chem. Soc. 2014, 136, 10974−10982

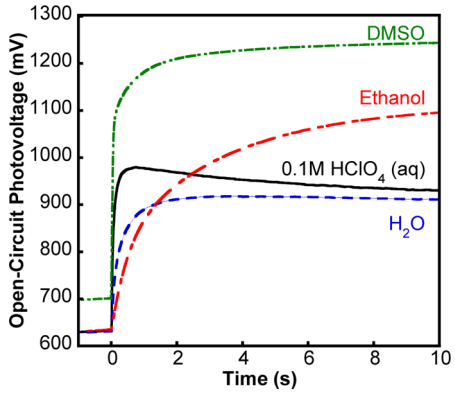

Figure 4. Representative photovoltages measured by chronopotentiometry under AM1.5 illumination. Electrodes were exposed to light at $t = 0$. (Γ_{uu}= (6−8) × 10^{-8} mol cm^{-2}).

photovoltages of electrodes prepared from DMSO and ethanol increase continuously and flatten out on a time scale of 10−20 s. The behavior of electrodes sensitized from 0.1 M $HClO_4$ (aq) is significantly different. In this case, the photovoltage peaks within one second and then falls off significantly over the next few few seconds. Electrodes sensitized from H_2O exhibit a slight decay in photovoltage after reaching their peak photovoltage, but the effect is not as pronounced as in the case of 0.1 M $HClO_4$ (aq). Following the model of Nelson et al.[34] as well as Salis et al.,[35] we can interpret the photovoltage decay in the 0.1 M $HClO_4$ (aq) and water cases as an indication that charge recombination ($e_{TiO_2} \rightarrow$ Ru(III)) or electron scavenging ($e_{TiO_2} \rightarrow$ Ir(IV)) is more rapid than reversible electron trapping/detrapping in the TiO_2 film. In contrast, the shape of the DMSO and ethanol curves suggests that reversible trapping/detrapping is competitive with recombination and electron scavenging.

The magnitude of the open-circuit photovoltage under 1 sun illumination is also quite different for the protic and aprotic deposition solvents. Electrodes sensitized from DMSO and ethanol have steady state photovoltages, 1101 ± 20 mV and 1049 ± 33 mV respectively, in agreement with previously reported values.[26] The photovoltages are significantly lower for electrodes sensitized from water (863 ± 23 mV) and 0.1 M $HClO_4$ (aq) (935 ± 30 mV).

We can rationalize these differences in the context of surface protonation and proton intercalation into TiO_2. The adsorption and intercalation of small cations is known to lower the open-circuit photovoltage in dye-sensitized solar cells by shifting the conduction band edge of TiO_2 to more positive potentials.[36] Lyon and Hupp[5] found a dependence of the conduction band potential on proton concentration that they ascribed to proton intercalation into TiO_2. Although this model suggests that electrodes senstized from 0.1 M $HClO_4$ (aq) should show the lowest photovoltage, surface protonation may mitigate the effect of proton intercalation through rapid cross-surface hole transport or higher injection yields. Emission spectra recorded at negative applied bias (−1.0 V vs Ag/AgCl, Figure S7, Supporting Information) show less residual emission for electrodes sensitized from 0.1 M $HClO_4$ (aq).

The gradual drop in photovoltage observed for films prepared from 0.1 M $HClO_4$ (aq) is consistent with the slow intercalation of protons into TiO_2. Intercalated protons produce shallow, long-lived (>10 ms) electrostatic trap states,[7] functionally acting as electron scavengers. Chemically, intercalated protons stabilize Ti(III) centers,[5] which act as near-surface recombination sites for electrons and result in lower open-circuit voltages.[37] Both effects would be consistent with a decay in the photovoltage over the time scale of tens of seconds.[34,35]

Spectroelectrochemistry. In order to test the hypothesis of proton intercalation, spectroelectrochemical measurements were performed. Ti(III) has a characteristically broad absorption across the visible and near-IR region.[38] Stepping in 100 mV increments from 0 V to −1.7 V vs Ag/AgCl (3 M NaCl), an increase in absorption past 500 nm that extends into the near-IR can be observed at potentials more negative than −0.8 V vs Ag/AgCl (Figure 5, top). In pH 6.8 phosphate buffer,

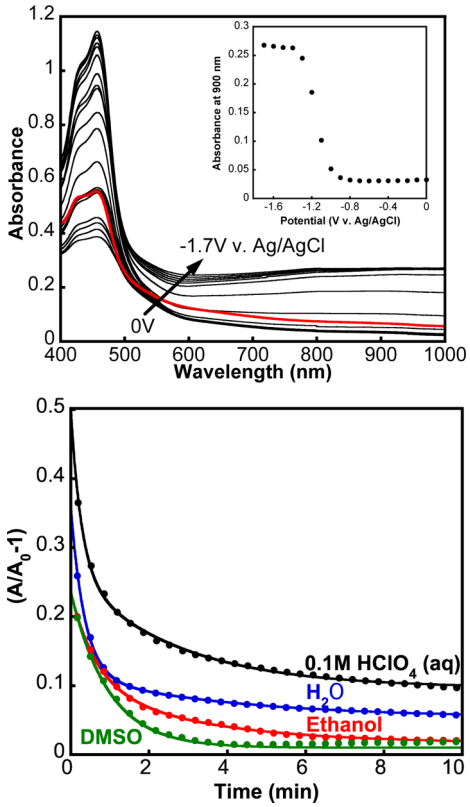

Figure 5. (Top) Absorption spectra of a TiO_2 electrode sensitized from an ethanol solution, with the potential stepped progressively from 0 to −1.7 V vs Ag/AgCl. After reaching −1.7 V, the circuit was opened for 30 min, and the last spectrum (red line) was recorded. (Bottom) Transient absorbance (900 nm) of sensitized electrodes held 5 min at −1.6 V vs Ag/AgCl before opening the circuit at time zero. Experimental data (closed cirles) were fit to single or biexponential decays (solid lines).

the conduction band of anatase TiO_2 is at approximately −0.81 V vs Ag/AgCl, consistent with the idea that the broad visible/near-IR absorbance is due to electrons in the conduction band, i.e., Ti(III) sites. Under open circuit conditions, this absorbance decays significantly within 10 min. No further decrease in absorption was observed after 20 or 30 min. We can ascribe the persistent change in absorbance to the persistence of protonated Ti(III) sites under open circuit conditions.

The formation and decay of proton-stabilized Ti(III) trap sites was studied for electrodes sensitized from DMSO, ethanol, water, and 0.1 M $HClO_4$ (aq) (Figure 5, bottom). These electrodes were held at −1.6 V vs Ag/AgCl for 5 min, the

dx.doi.org/10.1021/ja5040705 | J. Am. Chem. Soc. 2014, 136, 10974−10982

circuit was opened by disconnecting the working electrode lead, and the change in absorbance at 900 nm was monitored for 10 min. The decay curves were then fit to a biexponential of the form

$$\left(\frac{A}{A_0} - 1\right) = A_1 e^{-\tau_1/t} + A_2 e^{-\tau_2/t} + c \quad (3)$$

except for the DMSO-sensitized electrode, which was fit to a single exponential (Table S1, Supporting Information). The DMSO electrode exhibited the most rapid decay in absorbance (τ = 54 s) and had little residual absorbance (1.6%) at 900 nm after 10 min. The electrode sensitized in ethanol had a biexponential decay and the same small residual absorbance at the end of the experiment. In contrast, electrodes sensitized from water and $HClO_4$ (aq) had residual absorbances of 5 and 10%, respectively. The increase in residual absorbance with increasing acidity supports the notion of proton intercalation and stabilization of long-lived Ti(III) centers under acidic conditions.

Steady-State Photoelectrolysis. Photoanodes modified with sintered IrO_2 (50 pmol/cm^2)[26] were sensitized with [Ru(bpy)$_2$(4,4′-(PO$_3$H$_2$)$_2$bpy)] from each of the four solvents and studied in WS-DSPECs. We have previously determined that the Coulombic efficiency for oxygen evolution at these photoanodes is close to unity,[26] which is consistent with other measurements of oxygen and hydrogen yields in WS-DSPECs.[2,8,13] As is commonly observed in WS-DSPECs, the photocurrent rapidly decayed under illumination, though a portion of the photocurrent could be restored by holding the electrodes under open circuit conditions in the dark for a few seconds.[2,11,13,39] By a large margin, IrO_2-modified photoanodes sensitized from ethanol reached the highest peak current and passed significantly more current than electrodes prepared from the other solvents. Figure 6 shows that the ethanol-functionalized electrode briefly surpassed 206 μA/cm^2 before polarizing to ~40 μA/cm^2 after 10 min of illumination. Interestingly it takes 800 ms of illumination for the electrode sensitized from ethanol to reach its peak current before polarizing.

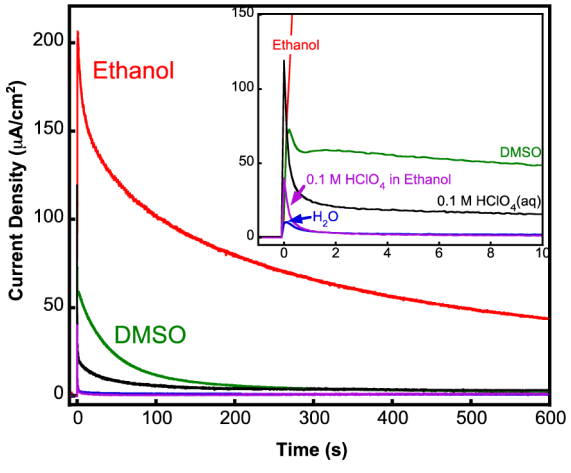

Figure 6. Representative bulk photoelectrolysis curves of photoanodes sensitized with [Ru(bpy)$_2$(4,4′-(PO$_3$H$_2$)$_2$bpy)] from different solvents. Catalyst loading is 0.50 pmol/cm^2 sintered IrO_2. Electrodes were biased at +100 mV vs Ag/AgCl (3 M NaCl) in 100 mM pH 6.8 NaH_2PO_4/Na_2HPO_4. The counter electrode was Pt mesh. Inset shows the first 10 s of the photoelectrolysis curves.

Similarly, after several hundred milliseconds of illumination, the electrode sensitized from DMSO reaches a peak current of 73 μA/cm^2 before polarizing. In the electrodes sensitized from protic solvents, the peak current was reached in less than 100 ms (the limit of resolution of the measurement) and rapidly polarized over the first second of illumination. Sensitizing from 0.1 M $HClO_4$ (aq) produces a peak current of 119 μA/cm^2, although after 1 s the current dropped to 24 μA/cm^2. The electrodes sensitized from water had the lowest peak current (11 μA/cm^2) and negligible current after 10 min. To determine if acidity played a role in lowering the photocurrent, electrodes were sensitized from 0.1 M $HClO_4$ in ethanol. As in the case of the 0.1 M $HClO_4$ (aq) samples, the peak current was reached immediately upon illumination and over the course of 500 ms polarized from 40 μA/cm^2 to less than 10 μA/cm^2.

In the anode of a DS-WSPEC, holes are transported across the TiO_2 surface by a series of lateral transfers between dye molecules (xi in Scheme 1). Water oxidation occurs when holes

Scheme 1. Electron Transfer Processes and Proton Intercalation in WS-DSPECs[a]

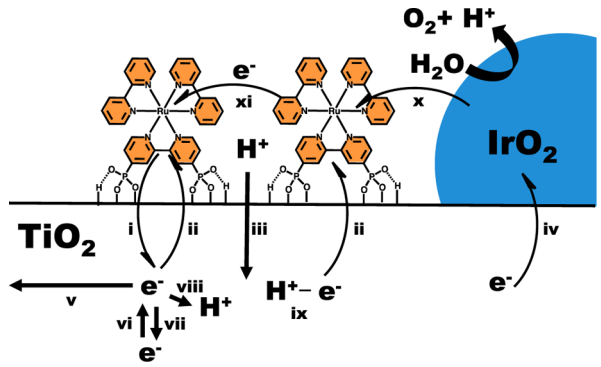

[a](i) injection, (ii) recombination, (iii) proton intercalation, (iv) electron scavenging by IrO_2, (v) electron transport to FTO, (vi,vii) reversible detrapping/trapping, (viii) trapping of an electron at a proton-stabilized site, (ix) proton-stabilized trap state, (x) regeneration of Ru(III) by IrO_2, (xi) cross-surface hole transport.

are transported to an IrO_2 catalyst particle. Alternatively, the hole may recombine with an electron from the TiO_2 conduction band, and photoinjected electrons may also be scavenged by IrO_2 catalyst particles (iv in Scheme 1).[26] These parasitic recombination pathways compete with the transport of electrons to the FTO-glass electrode through a trapping/detrapping process (vi and vii in Scheme 1) in the TiO_2 film. These processes are summarized pictorially in Scheme 1.

Because recombination (ii in Scheme 1) occurs on a time scale of hundreds of microseconds,[13] the rate of lateral hole transport is an important factor in determining the efficiency of WS-DSPECs. Films sensitized from ethanol have a higher value of D_{app} than those sensitized from water or DMSO. Broadly, the photocurrent (Figure 6) follows these trends, with ethanol-sensitized films showing higher photocurrent than electrodes sensitized from water or DMSO. This picture is clearly incomplete as films sensitized from 0.1 M $HClO_4$ (aq) have the highest value of D_{app} but very low photocurrent. Because these electrodes have the highest concentration of intercalated protons (iii in Scheme 1), recombination (with electrons in proton-stabilized Ti(III) centers, xi in Scheme 1) may be faster than it is with electrodes sensitized from nonaqueous solvents. This hypothesis is borne out in a kinetic analysis below.

dx.doi.org/10.1021/ja5040705 | J. Am. Chem. Soc. 2014, 136, 10974−10982

Similarly, the value of D_{app} calculated for water-sensitized films is 1 order of magnitude higher than that for DMSO, but the photocurrent produced by electrodes sensitized from DMSO is much greater.

We cannot exclude the possibility that injection efficiency or electrode stability may be affected by surface protonation for sensitizers deposited from 0.1 M $HClO_4$(aq). Qu and Meyer found an enhancement in the rates of both injection and recombination with surface protonation.[27] Nevertheless, it appears that proton intercalation plays a more dominant role in controlling the photoelectrochemistry.

We note that the decrease in photocurrent observed here when sensitizing from protic solvents is not observed with conventinal DSSCs.[28,40−42] The difference is related to the mechanism of dye regeneration. In DSSCs, regeneration of the oxidized dye by I^- is much faster than back electron transfer from TiO_2 to the oxidized dye. Thus, near-surface trapping of electrons in proton-stabilized Ti(III) (viii in Scheme 1) states is less deleterious to the performance of conventional DSSCs.[43]

Photocurrent Modeling. The kinetics of electron transfer sketched in Scheme 1 may be modeled quantitatively by following the approach of Nelson et al.[34] To simplify the model we assumed that electron recombination with oxidized [Ru(bpy)$_2$(4,4′-(PO$_3$H$_2$)$_2$bpy)] as well as scavenging by Ir(IV) occurs from the conduction band edge, which has energy E_c. On the basis of the light flux and coverage of the sensitizer, we calculated a generation rate (G) of approximately 10^{19} cm^{-3} s^{-1}. In this model the change in number density of conduction band electrons (n_{cb}) is determined by the rates of generation, detrapping, trapping, recombination with Ru(III), and scavenging by Ir(IV):

$$\frac{\partial n_{cb}}{\partial t} = G + k_{detrap} e^{-\frac{E_c - E_t}{kT}} (N_{cb} - n_{cb}) n_t - k_{trap} n_{cb} (N_t - n_t) - k_{recomb} n_{Ru^{3+}} n_{cb} - k_{scav} n_{Ir^{4+}} n_{cb} \quad (4)$$

Here k_{detrap}, k_{trap}, k_{recomb}, and k_{scav} are rate constants for detrapping, trapping, recombination with Ru(III), and scavenging by Ir(IV), respectively. The density of conduction band and trap states is given by N_{cb} and N_t respectively, and n_t is the number density of electrons in trap states. To further simplify the model, the energy of the trap states is given by a single value, E_t, rather than by an exponential distribution. The rate of change in the density of trapped electrons is simply described as the balance between trapping and detrapping:

$$\frac{\partial n_t}{\partial t} = k_{trap} n_{cb} (N_t - n_t) - k_{detrap} e^{-\frac{E_c - E_t}{kT}} (N_{cb} - n_{cb}) n_t \quad (5)$$

The number density of oxidized sensitizer molecules is determined by the rates of generation, recombination, and regeneration by the catalyst (k_{regen}):

$$\frac{\partial n_{Ru^{3+}}}{\partial t} = G - k_{recomb} n_{Ru^{3+}} n_{cb} - k_{regen} n_{Ir^{4+}} n_{Ru^{3+}} \quad (6)$$

Finally, the photocurrent is given by

$$I = q n_{cb} \mu_{cb} F A \quad (7)$$

where q is the charge of an electron, μ_{cb} is the mobility of electrons in the conduction band, F is the electric field across the electrode, and A is the area of the electrode. We take the electron mobility[34] to be 5×10^{-6} cm^2 V^{-1} s^{-1}. We estimate a potential drop of ∼100 mV across the TiO_2 film corresponding to an electric field of 83 V cm^{-1}.

The first 25 s of photocurrent for electrodes prepared from ethanol and DMSO fit well to the kinetic model (Figure 7).

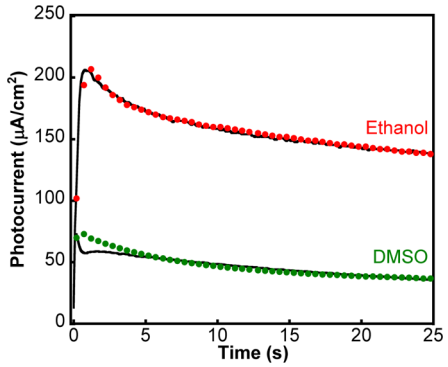

Figure 7. Photocurrent generated by DMSO (green circles) and ethanol-sensitized electrodes (blue circles) from Figure 6. Black lines represent modeled photocurrent. 20% of the data points are displayed to show the fit to the data.

Most notably, the model revealed a difference in k_{recomb} for ethanol vs DMSO (2.2×10^{-19} cm^{-3} s^{-1} vs 7.5×10^{-18} cm^{-3} s^{-1}). This can be explained by the poor hole transport characteristics (not considered explicitly in the model but reflected in k_{recomb}) of electrodes prepared from DMSO. Electrodes sensitized from ethanol also exhibited more rapid trapping and detrapping. The rate constant of electron scavenging by IrO_2, k_{scav}, we determine from the model (10^{-19} cm^3 s^{-1}) is very consistent with an independently measured value of 3.8×10^{-19} cm^3 s^{-1}.[26] We have also experimentally probed recombination between the oxidized dye and conduction band electrons.[13,26] Assuming that 0.01% of the sensitizer is oxidized at any time, we can estimate k_{recomb} from those studies to be between 10^{-18} and 10^{-20} cm^3 s^{-1}, which is again in good agreement with the values derived from the kinetic model.

Figure 8 shows the number density of n_{cb}, n_t, and Ru(III) from the photocurrent model of ethanol-sensitized electrodes. As expected, the shape of the n_{cb} curve mirrors the photocurrent (Figure 7). We see a steady increase in the density of trapped electrons until a steady state is reached at 1.33×10^{19} cm^3. In this state about 14% of the traps are filled.

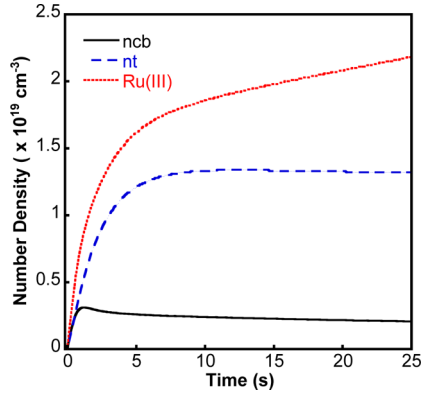

Figure 8. Calculated number density of conduction band electrons (n_{cb}), trapped electrons (n_t), and oxidized sensitizer molecules (Ru(III)) from photocurrent model of ethanol-sensitized electrode.

dx.doi.org/10.1021/ja5040705 | J. Am. Chem. Soc. 2014, 136, 10974−10982

The most important observation is the steadily increasing concentration of Ru(III) on the surface. Although this represents a tiny fraction of the dye coverage (≪1%), the buildup of Ru(III) plays a dominant role in the reversible polarization of the photocurrent over a time scale of tens of seconds. Slow regeneration of the oxidized dye has been proposed as a factor that limits the efficiency of WS-DSPECs and this is consistent with our model.

This simple model breaks down when we attempt to fit the photocurrent from electrodes sensitized in 0.1 M $HClO_4$ (aq) and water. Specifically, the model cannot reproduce the very rapid drop in photocurrent. Qualitatively, the model reaches maximum currently quickly and polarizes rapidly when the rates of recombination and scavenging by IrO_2 are 3 to 4 orders of magnitude greater than the rate of reversible trapping. However, even under these conditions, the immediate peak photocurrent and rapid polarization observed in Figure 6 are not reproduced. An additional term that describes long-lived proton-stabilized trap states improves the fit, but still cannot account for the observed shape of the photocurrent. It is also possible that our model is too simplistic and fails to account for another recombination pathway that is active with these electrodes.

Electrochemical Impedance Spectroscopy. Proton intercalation during photoelectrolysis is likely to occur in aqueous electrolytes as a charge compensation mechanism for photoinjected electrons. Lyon and Hupp[5] demonstrated that even in solvents with $-\log(a_{H^+}) = 23$, proton intercalation occurred to stabilize electrochemically generated Ti(III) sites. As noted above, proton intercalation acts both to lower the photovoltage and to create near-surface recombination centers for photoinjected electrons. Thus, it is reasonable to consider if proton intercalation during the photoelectrolysis might contribute to the rapid polarization or slower decay of photocurrent that is typically observed in WS-DSPECs.

To probe this hypothesis, we used electrochemical impedance spectroscopy under zero current conditions, scanning from 1 MHz to 10 Hz. At frequencies below 10 Hz, V_{oc} gradually reduces indicating electrode instability. The changes in impedance behavior that occur upon intercalation of small cations into metal oxides have been well studied.[44,45] Figure 9 shows Nyquist plots of a freshly sensitized electrode prepared from ethanol, the same electrode degraded after 10 min of illumination at +100 mV vs Ag/AgCl, and an electrode freshly sensitized from 0.1 M $HClO_4$(aq). Each spectrum shows a wide, distorted semicircle centered around 500 Ω. This is likely related to electron transfer at the FTO-glass contact,[46,47] although at this time we cannot identify the specific combination of transport channels, i.e., TCO to TiO_2 and/or TCO to electrolyte. In addition, the distortion of the semicircle may be related to the large area of the electrode.

Beyond the high frequency semicircle, the fresh electrode exhibits a second smaller semicircle that may be related to a recombination process from electrons in trap states.[46] With 0.1 M $HClO_4$ (aq) sensitized and degraded electrodes the behavior is markedly different. The spectra exhibit a slight curvature before an inflection point after which the plot becomes linear. This behavior is diagnostic of small cation diffusion within a solid lattice.[48]

In the idealized case of ordinary diffusion through a sold film, Warburg behavior is observed at frequencies higher than some characteristic diffusion frequency, ω_d. At frequencies lower than ω_d, a capacitive branch that is related to the charge stored by

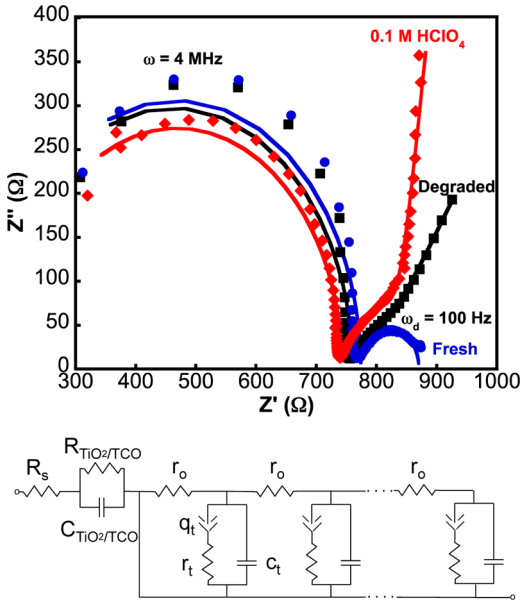

Figure 9. (Top) Nyquist plot of fresh ethanol-sensitized electrode (blue circles); an identical electrode degraded by photoelectrochemical testing at +100 mV vs Ag/AgCl under illumination (black circles); and an electrode freshly sensitzed from 0.1 M $HClO_4$ (aq) (red circles). Solid lines are fits to a simple transmission line equivalent circuit (bottom).

intercalated protons is observed.[44] A more realistic picture assumes that ions encounter shallow and deep trap sites as they diffuse through the electrode film. In this model, at $\omega > \omega_d$, the resistance associated with trapping (r_t) couples with a fast capacitance (c_t) related to electronic charge equilibration, to give curvature before the capacitive branch. At frequencies lower than ω_d, transitions from deep to shallow trap states are more likely, which is reflected in a vertical increase in capacitance.[48] A weakness of this analysis is that it assumes only two types of trap states, shallow and deep. A more realistic model would allow for a distribution of trap state energies. The slow capacitance associated with trapping is thus replaced by a constant phase element (q_t) that models a distribution of energies. The index (γ) of the constant phase element describes the energetic distribution of trap states, with γ =1 corresponding to the simple distribution described above.[45] In the Nyquist plot, the slope of the linear ion diffusion capacitance is determined by γ. When γ =1, the capacitive branch is perfectly vertical with infinite slope.

The capacitive branches in the Nyquist plot of the 0.1 M $HClO_4$ (aq) sensitized and degraded electrodes exhibit the features associated with trapping-limited transport through an energy-dispersive landscape of traps. To explore this further we attempted to fit the impedance spectra in Figure 9 to a series of simple transmission line circuits. The bottom of Figure 9 shows a single rail transmission line, with transport in TiO_2 and transport in the electrolyte ignored. However, we also explored models with transport exclusively in the electrolyte as well as several mixed transmission combinations. No model provided an especially close fit to the high frequency semicircles and the parameters associated with that portion of the spectra were very sensitive to change. This is unsurprising as we do not have a detailed understanding of the physical model that generates that semicircle. With the $HClO_4$ (aq) sensitized and degraded electrodes, all models that we tested gave excellent fits to the

dx.doi.org/10.1021/ja5040705 | J. Am. Chem. Soc. 2014, 136, 10974−10982

capacitive branches of the spectra with very similar values of interfacial impedances. For 0.1 M $HClO_4$ (aq), C_t was approximately 20−30 μF, $R_t \sim$ 210−220 Ω, $Q_t \sim 1.0-3.0 \times 10^{-5}\ \Omega^{-1}$, and $\gamma \sim 0.8$ to 0.9. For the degraded electrode C_t was approximately 35−45 μF, $R_t \sim$ 375 to 405 Ω, $Q_t \sim$ 6.6 to 15.1 $\times 10^{-5}\ \Omega^{-1}$, and $\gamma \sim$ 0.66 to 0.72. We posit that the quality of the fit and the relative insensitivity to the rest of the model suggests that we have appropriately modeled the capacitive branch of the Nyquist plot as an ion intercalation and diffusion process. The freshly sensitized ethanol electrode did not fit well to the model incorporating ion diffusion through the lattice. Instead the spectrum was fit well to the simple interfacial capacitance model described by a resistor and capacitor in parallel.[47]

The distinct capacitive branches observed in the degraded and 0.1 M $HClO_4$ (aq) sensitized electrodes most likely describe intercalated proton diffusion through the TiO_2 lattice. As this feature is not observed in the freshly sensitized electrode, we conclude that proton intercalation occurs slowly during photoelectrolysis. Furthermore, on the basis of the substantial decrease in photocurrent and photovoltage that results from sensitization under acidic conditions, we suggest that proton intercalation plays a significant role in the long term degradation of the photovoltage and photocurrent. This is consistent with previous results,[36,49] which demonstrate that ion intercalation moves the conduction band potential to more positive potentials and increases the rate of recombination (Scheme 1).

It is important to note that this proton intercalation is not likely to arise from inadequate buffering within the electrode. At the low current density of the WS-DSPEC, the diffusion of buffering ions should be substantially faster than the rate of proton generation, so little change in local pH within the electrode is expected (see Supporting Information). Thus, proton intercalation during photoelectrolysis is not due to high local acidity generated by photoelectrochemical water oxidation, although this effect could become more important for efficient electrodes that generate an order of magnitude higher photocurrent density.[5]

CONCLUSION

The choice of dye deposition solvent has a significant effect on the performance of WS-DSPECs, despite the fact that they are tested in identical buffered aqueous media. The acidity of the solvent appears to affect the degree of sensitizer aggregation on the TiO_2 surface as well as the rate of cross-surface hole diffusion.

Although lateral hole transport is an important factor in the efficiency of WS-DSPECs, we find that electrodes sensitized from 0.1 M $HClO_4$ (aq) exhibit low photocurrent and low open-circuit voltages, despite their high values of D_{app}. Qualitatively the shapes of both the photocurrent and open-circuit voltage decay curves suggest that charge recombination is very fast in this case. Conversely, electrodes prepared from neat ethanol and DMSO exhibit higher photocurrents and more closely fit a model in which reversible trapping/detrapping in sub-bandgap states is kinetically competitive with recombination and electron scavenging. Fits to this model show the key role of trapped electrons in limiting the photocurrent and causing electrode polarization, effects that are not seen in conventional DSSCs where dye regeneration is typically very fast. This suggests that electrode architectures that speed up electron transport to the FTO/glass surface could be effective in increasing the efficiency of WS-DSPECs, even though they have not been very effective with conventional DSSCs.

A reasonable hypothesis for the difference in behavior between electrodes prepared in nonaqueous and acidic aqueous solvents involves the formation of long-lived proton-stabilized trap sites. Chemically, these traps are protonated Ti(III) sites, which can act as near-surface recombination centers. We find spectroelectrochemical evidence for a higher density of these trap states in electrodes sensitized from 0.1 M $HClO_4$ (aq) than in electrodes sensitized from nonaqueous solvents.

Finally, we considered proton intercalation effects during photoelectrolysis to gain insight into the slow degradation of electrodes sensitized from nonaqueous solvents. Electrochemical impedance spectra of electrodes degraded by illumination at +100 mV vs Ag/AgCl and electrodes freshly sensitized from 0.1 M $HClO_4$ (aq) exhibit distinct capacitive branches that can be attributed to proton diffusion through the TiO_2 lattice. As these capacitive branches do not appear in freshly ethanol sensitized electrodes, we conclude that proton intercalation can occur during photoelectrolysis and contributes to the degradation process.

ASSOCIATED CONTENT

Supporting Information

Sensitizer adsorption isotherms; cyclic voltammetry of electrodes sensitized from DMSO and H_2O; current−time data used to obtain D_{app} values; fit parameters for curves in Figure 5; photocurrent model fit parameters for DMSO and ethanol in Figure 7; analysis of buffering and diffusion in WS-PECs; emission data from electrodes at negative applied bias (6 pp). This material is available free of charge via the Internet at http://pubs.acs.org.

AUTHOR INFORMATION

Corresponding Author

tem5@psu.edu

Notes

The authors declare no competing financial interest.

ACKNOWLEDGMENTS

The authors thank Dunwei Wang and Nella Vargas-Barbosa for helpful discussions. We thank Ben Lear for assistance with FTIR measurements. This work was supported by the Office of Basic Energy Sciences, Division of Chemical Sciences, Geosciences, and Energy Biosciences, Department of Energy under Contract DE-FG02-07ER15911. N.S.M. thanks the National Science Foundation for support as a graduate fellow under Grant DGE1255832. Instrumentation and facilities used in this project were supported by the Pennsylvania State University Materials Research Institute Nanofabrication Laboratory under National Science Foundation Cooperative Agreement ECS-0335765.

REFERENCES

(1) Swierk, J. R.; Mallouk, T. E. *Chem. Soc. Rev.* **2013**, *42*, 2357−2387.

(2) Gao, Y.; Ding, X.; Liu, J.; Wang, L.; Lu, Z.; Li, L.; Sun, L. *J. Am. Chem. Soc.* **2013**, *135*, 4219−4222.

(3) Berger, T.; Lana-Villarreal, T.; Monllor-Satoca, D.; Gomez, R. *J. Phys. Chem. C* **2007**, *111*, 9936−9942.

(4) Solbrand, A.; Lindström, H.; Rensmo, H.; Hagfeldt, A.; Lindquist, S.-E.; Södergren, S. *J. Phys. Chem. B* **1997**, *101*, 2514−2518.

(5) Lyon, L. A.; Hupp, J. T. *J. Phys. Chem. B* **1999**, *103*, 4623−4628.
(6) Savory, D. M.; McQuillan, A. J. *J. Phys. Chem. C* **2013**, *117*, 23645−23656.
(7) Halverson, A. F.; Zhu, K.; Erslev, P. T.; Kim, J. Y.; Neale, N. R.; Frank, A. J. *Nano Lett.* **2012**, *12*, 2112−2116.
(8) Lee, S.-H. A.; Zhao, Y.; Hernandez-Pagan, E. A.; Blasdel, L.; Youngblood, W. J.; Mallouk, T. E. *Faraday Discuss.* **2012**, *155*, 165−176.
(9) Ardo, S.; Meyer, G. J. *J. Am. Chem. Soc.* **2010**, *132*, 9283−9285.
(10) Hanson, K.; Brennaman, M. K.; Ito, A.; Luo, H.; Song, W.; Parker, K. A.; Ghosh, R.; Norris, M. R.; Glasson, C. R. K.; Concepcion, J. J.; Lopez, R.; Meyer, T. J. *J. Phys. Chem. C* **2012**, *116*, 14837−14847.
(11) Youngblood, W. J.; Lee, S.-H. A.; Kobayashi, Y.; Hernandez-Pagan, E. A.; Hoertz, P. G.; Moore, T. A.; Moore, A. L.; Gust, D.; Mallouk, T. E. *J. Am. Chem. Soc.* **2009**, *131*, 926−927.
(12) Brimblecombe, R.; Koo, A.; Dismukes, G. C.; Swiegers, G. F.; Spiccia, L. *J. Am. Chem. Soc.* **2010**, *132*, 2892−2894.
(13) Zhao, Y.; Swierk, J. R.; Megiatto, J. D.; Sherman, B.; Youngblood, W. J.; Qin, D.; Lentz, D. M.; Moore, A. L.; Moore, T. A.; Gust, D.; Mallouk, T. E. *Proc. Natl. Acad. Sci. U. S. A.* **2012**, *109*, 15612−15615.
(14) Alibabaei, L.; Brennaman, M. K.; Norris, M. R.; Kalanyan, B.; Song, W.; Losego, M. D.; Concepcion, J. J.; Binstead, R. A.; Parsons, G. N.; Meyer, T. J. *Proc. Natl. Acad. Sci. U. S. A.* **2013**, *110*, 20008−20013.
(15) Hanson, K.; Brennaman, M. K.; Luo, H.; Glasson, C. R. K.; Concepcion, J. J.; Song, W.; Meyer, T. J. *ACS Appl. Mater. Interfaces* **2012**, *4*, 1462−1469.
(16) Moore, G.; Konezny, S.; Song, H.; Milot, R.; Blakemore, J. D.; Lee, M. L.; Batista, V. S.; Schmuttenmaer, C. A.; Crabtree, R. H.; Brudvig, G. W. *J. Phys. Chem. C* **2012**, *116*, 4892−4902.
(17) Moore, G. F.; Blakemore, J. D.; Milot, R. L.; Hull, J. F.; Song, H.-E.; Cai, L.; Schmuttenmaer, C. A.; Crabtree, R. H.; Brudvig, G. W. *Energy Environ. Sci.* **2011**, *4*, 2389−2392.
(18) Nelson, J. *Phys. Rev. B: Condens. Matter Mater. Phys.* **1999**, *59*, 15374−15380.
(19) van de Lagemaat, J.; Park, N. G.; Frank, A. J. *J. Phys. Chem. B* **2000**, *104*, 2044−2052.
(20) Adachi, M.; Sakamoto, M.; Jiu, J.; Ogata, Y.; Isoda, S. *J. Phys. Chem. B* **2006**, *110*, 13872−13880.
(21) J Frank, A.; Kopidakis, N.; Lagemaat, J. V. d. *Coord. Chem. Rev.* **2004**, *248*, 1165−1179.
(22) Benkstein, K. D.; Kopidakis, N.; van de Lagemaat, J.; Frank, A. J. *J. Phys. Chem. B* **2003**, *107*, 7759−7767.
(23) Bisquert, J.; Zaban, A. *Appl. Phys. A: Mater. Sci. Process.* **2003**, *77*, 507−514.
(24) Gillaizeau-Gauthier, I.; Odobel, F.; Alebbi, M.; Argazzi, R.; Costa, E.; Bignozzi, C. A.; Qu, P.; Meyer, G. J. *Inorg. Chem.* **2001**, *40*, 6073−6079.
(25) Lee, S.-H. A.; Abrams, N. M.; Hoertz, P. G.; Barber, G. D.; Halaoui, L. I.; Mallouk, T. E. *J. Phys. Chem. B* **2008**, *112*, 14415−14421.
(26) Swierk, J. R.; McCool, N. S.; Saunders, T. P.; Barber, G. D.; Strayer, M. E.; Vargas-Barbosa, N. M.; Mallouk, T. E. *J. Phys. Chem. C.* **2014**, DOI: 10.1021/jp500589n.
(27) Qu, P.; Meyer, G. J. *Langmuir* **2001**, *17*, 6720−6728.
(28) Kim, B.; Park, S. W.; Kim, J.-Y.; Yoo, K.; Lee, J. A.; Lee, M.-W.; Lee, D.-K.; Kim, J. Y.; Kim, B.; Kim, H.; Han, S.; Son, H. J.; Ko, M. J. *ACS Appl. Mater. Interfaces* **2013**, *5*, 5201−5207.
(29) Bae, E.; Choi, W.; Park, J.; Shin, H. S.; Kim, S. B.; Lee, J. S. *J. Phys. Chem. B* **2004**, *108*, 14093−14101.
(30) Bertrand, P.; Jonas, A.; Laschewsky, A.; Legras, R. *Macromol. Rapid Commun.* **2000**, *21*, 319−348.
(31) Bonhôte, P.; Gogniat, E.; Tingry, S.; Barbé, C.; Vlachopoulos, N.; Lenzmann, F.; Comte, P.; Grätzel, M. *J. Phys. Chem. B* **1998**, *102*, 1498−1507.
(32) Trammell, S. A.; Meyer, T. J. *J. Phys. Chem. B* **1999**, *103*, 104−107.
(33) Fillinger, A. *J. Electrochem. Soc.* **1999**, *146*, 4559.
(34) Nelson, J.; Eppler, A. M.; Ballard, I. M. *J. Photochem. Photobiol., A* **2002**, *148*, 25−31.
(35) Salis, M.; Anedda, A.; Quarati, F.; Blue, A. J.; Cunningham, W. *J. Appl. Phys.* **2005**, *97*, 033709.
(36) Fredin, K.; Nissfolk, J.; Boschloo, G.; Hagfeldt, A. *J. Electroanal. Chem.* **2007**, *609*, 55−60.
(37) Yu, Y.; Wu, K.; Wang, D. *Appl. Phys. Lett.* **2011**, *99*, 192104.
(38) Koelle, U.; Moser, J.; Graetzel, M. *Inorg. Chem.* **1985**, *24*, 2253−2258.
(39) Brimblecombe, R.; Koo, A.; Dismukes, G. C.; Swiegers, G. F.; Spiccia, L. *ChemSusChem* **2010**, *3*, 1146−1150.
(40) Wang, Z.-S.; Zhou, G. *J. Phys. Chem. C* **2009**, *113*, 15417−15421.
(41) Watson, D. F.; Marton, A.; Stux, A. M.; Meyer, G. J. *J. Phys. Chem. B* **2003**, *107*, 10971−10973.
(42) Wu, K.-J.; Shen, K.; Yu, Y.; Wang, D.-L. *Chin. J. Chem. Phys.* **2013**, *25*, 733−738.
(43) Boschloo, G.; Hagfeldt, A. *Acc. Chem. Res.* **2009**, *42*, 1819−1826.
(44) Bisquert, J.; Vikhrenko, V. S. *Electrochim. Acta* **2002**, *47*, 3977−3988.
(45) Fabregat-Santiago, F.; Garcia-Belmonte, G.; Bisquert, J.; Ferriols, N. S.; Bueno, P. R.; Longo, E.; Antón, J. S.; Castro-García, S. *J. Electrochem. Soc.* **2001**, *148*, E302.
(46) Wang, Q.; Moser, J. E.; Grätzel, M. *J. Phys. Chem. B* **2005**, *109*, 14945−14953.
(47) Fabregat-Santiago, F.; Bisquert, J.; Palomares, E.; Otero, L.; Kuang, D.; Zakeeruddin, S. M.; Grätzel, M. *J. Phys. Chem. C* **2007**, *111*, 6550−6560.
(48) Bisquert, J. In *New Trends in Intercalation Compounds for Energy Storage*; Julien, C., Pereira-Ramos, J. P., Momchilov, A., Eds.; Springer: Dordrecht, the Netherlands, 2002; pp 405−412.
(49) Fabregat-Santiago, F.; Barea, E. M.; Bisquert, J.; Mor, G. K.; Shankar, K.; Grimes, C. A. *J. Am. Chem. Soc.* **2008**, *130*, 11312−11316.